Structural, dielectric and energy storage properties of Neodymium niobate with tetragonal tungsten bronze structure

M. Belarbi, Y. Tamraoui, B. Manoun, A. Cantaluppi, Y. Gagou, K. Taibi, M. El Marssi, A. Lahmar

Structural, Dielectric and Energy Storage Properties of Neodymium Niobate with Tetragonal Tungsten Bronze Structure

M. Belarbi[a], Y. Tamraoui[b], B. Manoun[b, c], A. Cantaluppi[a], Y. Gagou[a], K. Taibi[d], M. El Marssi[a], A. Lahmar[a, *]

[a]*Laboratoire de Physique de la Matière condensée (LPMC), 33 Rue saint Leu, 80039 Amiens.*

[b]*Materials Science and Nano-engineering, Mohammed VI Polytechnic University Lot 660 Hay Moulay Rachid, Ben Guerir, Morocco.*

[c]*Université Hassan 1[er], Laboratoire Rayonnement-Matière et Instrumentation, S3M, FST Settat, Morocc.o*

[d] *Laboratoire de Cristallographie-Thermodynamique, Faculté de Chimie, Université des Sciences et de la Technologie Houari Boumediene, BP32, Al Alia, 16111, Algiers, Algeria.*

Abstract

The present work reports the effect of Nd^{3+} substitution on the structural, dielectric and energy storage properties of the polycrystalline $Ba_2NaNb_5O_{15}$(BNN) ceramics. The ferroelectric lead-free $Ba_2Na_{1-x}Nd_{x/3}Nb_5O_{15}$ ceramics were prepared by conventional solid-state reaction technique. The room temperature X-ray study and Raman spectroscopy investigations have allowed evidencing the stabilization of a tetragonal tungsten bronze structure with *P*4*bm* space group for all the studied compounds. Dielectric study carried out on the prepared ceramics has permitted to determine the temperature of phase transitions (T_c). It was found that the dielectric constant increased with increasing the amount of Nd in BNN matrix. Room temperature energy storage property was determined using *P-E* hysteresis loops. The optimum discharge density was found for the composition x= 0.7 with W_{rec} = 18.1 mJ.cm^{-3}) at 1Hz. Finally, the dynamic of phase transition was approached using thermal Raman spectroscopy investigations.

.

Keywords: Tetragonal Tungsten Bronze; Structure; Dielectric; Energy storage; Raman spectroscopy.

* corresponding author: abdel.ilah.lahmar@u-picardie.fr (A. Lahmar)

1. Introduction

Tetragonal tungsten bronze structural type (TTB) is recognized as an attractive ferroelectric family with interesting properties compatible with several applications in different fields like ferroelectricity [1-3], ferroelasticity [4,5] electro-optic [6], non-linear optic [7], elasto-optic [8], acousto-optic [9], FRAM [10,11] etc. Furthermore, the literature examination revealed that some rare-earth doped TTB-compounds have shown interest related to their diffuse phase transition [12-14] and to the emission in green and blue laser light [16-18].

Obviously, the corresponding general crystal chemical formula of TTB type compound is given as: $(A_1)_4(A_2)_2C_4(B_1)_8(B_2)_2O_{30}$, with B_1 and B_2 cations forming octahedral cavities arranged in the manner to delimit wide tunnels running parallel to [001], with three types of sections: pentagonal (A_1), square (A_2), and trigonal (C).

Noting that TTB structure allows a wide variety of compensating substitutions depending on the size of cations which should be located in the appropriate site of the lattice: large size ions like K^+ cations are located in the 15-fold co-ordinated cavities (A_1), medium size ions like Sr^{2+} cations will fill the 12-fold coordinated spheres (A_2) and very small size ions like Li^+ can rather easily occupy the 9-fold cavities (C). However, the latter cavities are rarely occupied as in the case of $K_6Li_4Nb_{10}O_{30}$ [19,20]. Furthermore, niobate and tantalate mixed oxides seem to be the most common compounds that give rise to such structural type where Nb(V) and Ta(V) cations are located in two different octahedral sites (B_1 and B_2). For many compounds containing medium size cations of different natures like Sr^{2+} and Ln^{3+} (rare earth element) the stoichiometry imposes a mixed site occupation [21]. A disordered occupation of A1, A2 and C cavities could then be expected.

It should be noticed, however, that $Ba_2NaNb_5O_{15}$ (BNN)is the most studied compound in the literature. This interest is motivated by the existence of successive phase transitions as well as by its potential use as a generator of a second harmonic of a laser beam at 0.53 µm. Recall that this phase is a particular composition of a solid solution of the tetragonal tungsten bronze structure (TTB) delimited by $Ba_{1.90}Na_{1.2}Nb_5O_{15}$ and $Ba_{2.27}Na_{0.46}Nb_5O_{15}$ compositions [22]. In fact, these two extreme phases are non-stoichiometric and vacancies constitute a part of the structure. $Ba_{2.27}Na_{0.46}Nb_5O_{15}$ phase contains 9% of vacancies due to the partial occupation of pentagonal and square sites. Furthermore, the BNN is a ferroelectric material that undergoes six phase transitions, with three incommensurate phases and a rare phase transition between two incommensurate phases [23]. Further, Cavailli *et al.*[24] reported that

BNN is affected by quasi-commensurate structural modulation produced by cooperative tilting of the NbO_6 octahedra, responsible for the reduction of the real symmetry from tetragonal to orthorhombic. This disturbs the structure homogeneity, which constitutes a serious drawback for applications. Foulon et al [16] reported that the incorporation of a small amount of Nd^{3+} in the BNN matrix induced a stabilization of the tetragonal phase and thus the suppression of the incommensurate phases. This new structural arrangement was found to be beneficial for efficient self-frequency doubling application.

In the present work, emphasis is placed on how the high concentration of Nd^{3+} affects the structural, dielectric, ferroelectric and energy storage properties of BNN matrix. Herein, we are primarily interested in the incorporation of Neodymium in the Na-sites (square sites) according to the solid solution $Ba_2Na_{1-x}Nd_{x/3}Nb_5O_{15}$ with $0<x\leq0.7$.

2.Experimental

Polycrystalline samples were elaborated using regular solid-state reaction. Appropriate amounts of the starting materials were directly reacted according to the stoichiometry of the following equation:

$$(1-x)\ Na_2CO_3 + 4\ BaCO_3 + x/3Nd_2O_3 + 5Nb_2O_5 \rightarrow 2Na_{(1-x)}Ba_2Nd_{x/3}Nb_5O_{15} + (5-x)\ CO_2$$

The starting mixture was thoroughly grounded and submitted to various heat treatments from 300 up to 1250°C. Room temperature powder x-ray diffraction patterns were recorded on a discover Brucker diffractometer (Cu Kα = 1.5406 Å) to check the phase purity and to confirm that it crystallises with the tetragonal tungsten bronze structural type. High temperature Raman investigation has been carried out on the ceramic samples within the temperature range 25–560°C using a micro-Raman Renishaw spectrometer with an argon laser excitation under a power of 20 mW. Dielectric measurements were performed within the temperature range- 30 to 600°C, using ceramic capacitors made by sintered disks with parallel faces painted with silver paste. The energy storage property was investigated based on the *P*–*E* hysteresis loops recorded using a ferroelectric tester (TF Analyzer 3000) at ambient temperature and at the frequency of 1 Hz.

3. Results and Discussion

3.1. Microstructural analysis

An analysis by scanning electron microscopy was carried out on all the investigated samples. The micrographs presented in Figure 1, show the evolution of the microstructure and the grain

morphology versus Nd- element doping. As it can be depicted from the images, the free BNN shows a dominant rectangular grain (Fig1.a). The incorporation of Nd in the host lattice induced a change of the grain shape. Furthermore, the average grain size of the ceramic seems to decrease and becomes more uniform when the substitution rate increases (Figs.1 (b) and (c)). However, at x = 0.7 Nd^{3+} concentration, a coalescence and welding of grains are clearly observed.

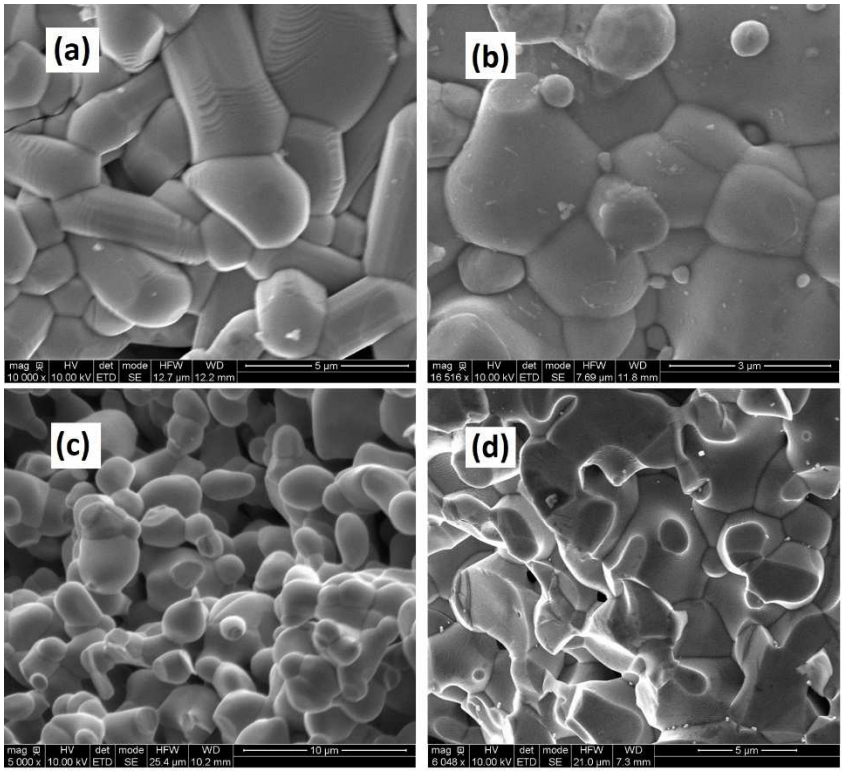

Figure.1. SEM micrographs of $Ba_2Na_{(1-x)}Nd_{x/3}Nb_5O_{15}$ solid solution: (a)x=0, (b) x=0.3,(c) x=0.5,(d)x=0.7

3.2. Crystal structure investigation

Figure 2 shows the typical Rietveld refinement x-ray patterns along with the difference plot at ambient temperature for $Na_{1-x}Nd_{x/3}Ba_2Nb_5O_{15}$ (x = 0.3, 0.5, 0.7). Noting that using the computer program Dicvol [25], an indexing of X-ray powder diffraction patterns was performed satisfactorily for these compositions. All diffraction patterns show a single phase with tetragonal bronze type structure and space group (*P4bm N° 100)*. No additional or intermediate phases were detected for the compositions x=0.3 and 0.5. The impurity $BaNb_2O_6$ (a= 12.205768, b= 10.277569, c= 7.864460) was detected for x=0.7. There is no remarkable decrease in the shift of 2θposition as substituting Na^+ (1.39 Å) by Nd^{3+} (1.27 Å) [26]. The lattice parameters that were refined using the complete powder diffraction data sets are listed in table 1. As can be seen from the table, there is a gradual decrease in the a(Å) parameter and

the volume as the amount of Nd^{3+} increases, however for *c* (Å) parameter a remarkable increase is observed with Nd^{3+}content.

Furthermore, the x-ray powder patterns were fitted to the calculated ones using a full-profile analysis program (FullProf) [27, 28] to minimize the profile discrepancy factor *Rp*. For $Na_{1-x}Nd_{x/3}Ba_2Nb_5O_{15}$, the refinement of the powder XRD patterns were carried out with tetragonal (*P*4*bm*) model. In this model Ba^{2+} and Na^{+}/Nd^{3+} cations are placed at 4*c* (*x*, *x*+1/2, *z*), Na^{+}/Nd^{3+} and 2*a* (0, 0, *z*) sites respectively; Nb^{5+} cations occupy the sites 8d(*x*, *y*, *z*) and 2*b*(0, 0.5, *z*) sites, and the oxygen atoms occupy the 8*d* Wyckoff positions (*x*, *y*, *z*), 4*c*(*x*, *x*+1/2,*z*) and 2*b*(0, 0.5, *z*). For all the investigated compounds, the refinements of the occupancies of all atoms show no significant deviation from their stoichiometric values. Significantly, good residuals of the refinements are obtained (see figure 2). The refined position coordinates are given in table 2 and the selected interatomic distances are listed in table 3.

The analysis of the refined crystallographic parameters of the studied compositions indicates that $Nb^{5+}$are coordinated by 6 oxygen atoms in an octahedral configuration with Nb–O distances varying from 1.93 to 2. 06Å.The (Ba^{2+}) and (Na^{+}/Nd^{3+}) in the site 4*c* and 2*a* have a coordination number of 15 and 12 respectively as shown in figure 3 for $Na_{0.7}Nd_{0.1}Ba_2Nb_5O_{15}$ chosen as an example. Figure 3(a) shows one lattice configuration in (a, b) plane projection and Figure 3(b) shows 3D atomic positions in between structural sharing octahedral framework.

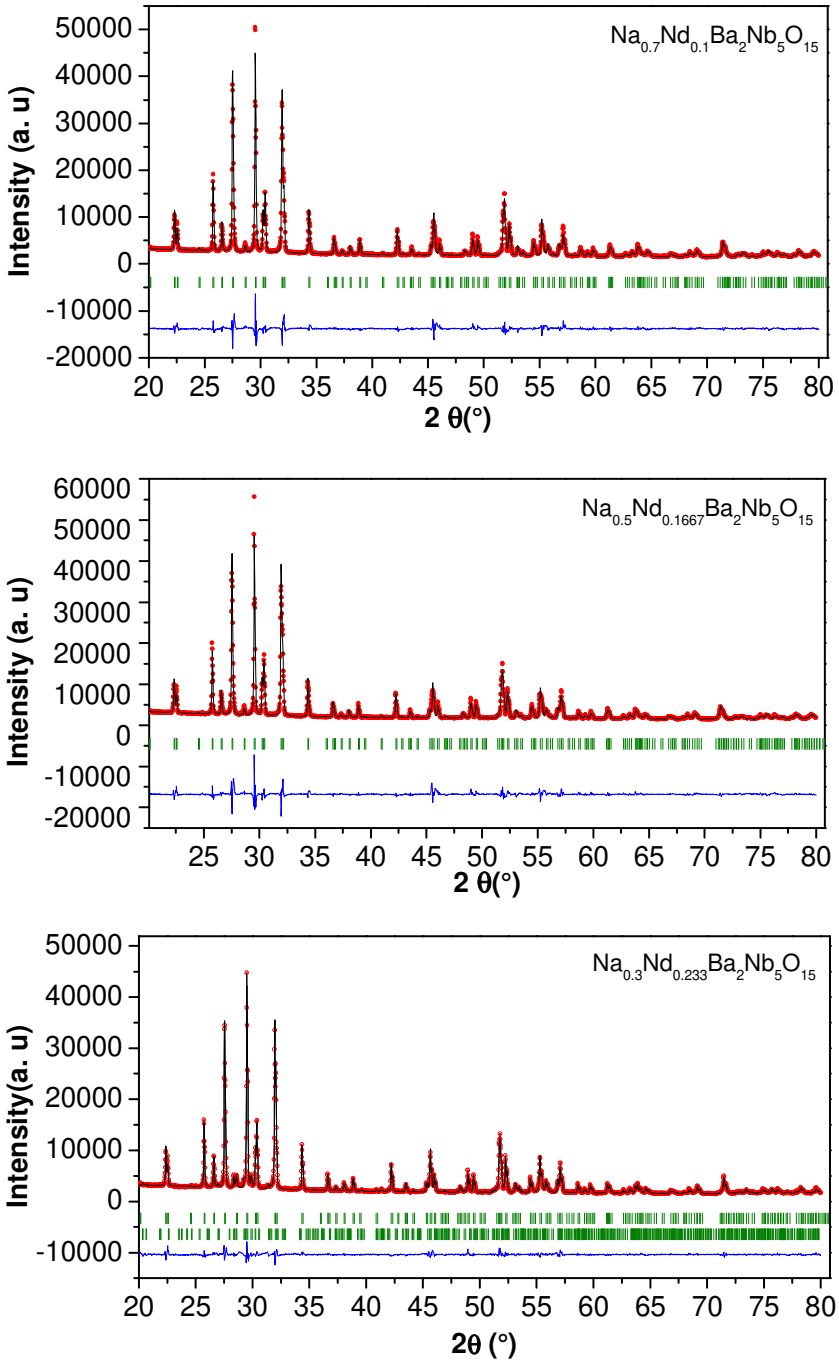

Figure 2. *Plot of Rietveld refinement of the series* $Na_{1-x}Nd_{x/3}Ba_2Nb_5O_{15}$ *(x= 0.3, 0.5 and 0.7). The composition* $Na_{0.3}Nd_{0.233}Ba_2Nb_5O_{15}$ *was fitted with the orthorhombic* $BaNb_2O_6$ *as an impurity (a= 12.2058, b= 10.2776, c= 7.8645). The upper symbols illustrate the observed data (red circles) and the calculated pattern (solid line). The vertical markers show calculated positions of the Bragg reflections. The lower curve is the difference diagram.*

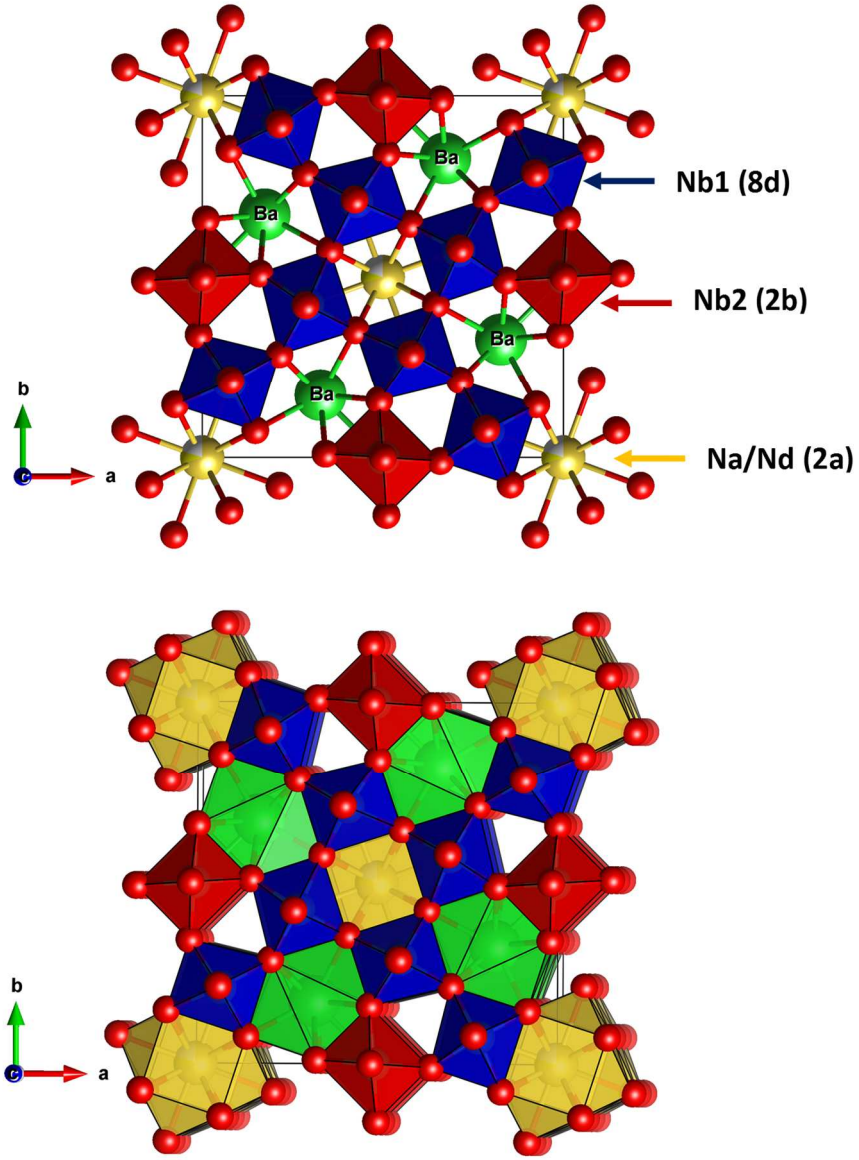

Figure 3. *Schematic representation of structure view of* $Na_{0.7}Nd_{0.1}Ba_2Nb_5O_{15}$.

Table 1 *Details of Rietveld refinement conditions of the series* $Na_{1-x}Nd_{x/3}Ba_2Nb_5O_{15}$

Composition	**$Na_{0.7}Nd_{0.1}Ba_2Nb_5O_{15}$**	**$Na_{0.5}Nd_{0.1667}Ba_2Nb_5O_{15}$**	**$Na_{0.3}Nd_{0.233}Ba_2Nb_5O_{15}$**
Symmetry	tetragonal	tetragonal	tetragonal
Space group	*P4bm*	*P4bm*	*P4bm*
Z	2	2	2
Lattice parameters (Å)	*a*=*b*= 12.4606(1) *c*= 3.9821(1)	*a*=*b*= 12.4621(7) *c*= 3.9783(2)	*a*=*b*= 12.4722(1) *c*= 3.9714(1)
Volume	618.302(2)	617.858(7)	617.773(2)
P-V function	0.71621(3)	0.65310(7)	0.76212(5)
Caglioti parameters	*U*= 0.1471(7) *V*=-0.0692(5) *W*= 0.0144(4)	*U*= 0.2061(9) *V*= -0.1050(1) *W*=0.0204(1)	*U*= 0.0855(4) *V*= -0.0437(3) *W*= 0.0105(6)
R_F/R_B	4.38 /5.88	4.88/6.83	2.51/3.50
R_P/R_{wp}	4.75/6.82	5.55/ 8.10	3.33/4.54
cR_P/cR_{wp}	4.75/6.82	5.55/8.10	3.33/4.54

Table 2 *Refined structural parameters for* $Na_{1-x}Nd_{x/3}Ba_2Nb_5O_{15}$ *with P4bm as space group.*

	Site	*x*	*y*	*z*	Biso	Occupancy
x= 0.3	**$Na_{0.7}Nb_{0.1}Ba_2Nb_5O_{15}$**					
Ba	4*c*	0.1728(6)	0.6728(7	0.1888(2	0.7099(5)	2
Na/Nd	2*a*	0	0	0.1783(7)	0.7099(5)	0.7/0.1
Nb1	8*d*	0.0738(7)	0.2094(6)	0.7027(5)	0.7099(5)	4
Nb2	2*b*	0.000	0.5	0.6989(2)	0.7099(5)	1
O1	8*d*	0.0127(9)	0.6560(1)	0.7650(7)	1.9578(7)	4
O2	8*d*	0.0738(1)	0.8511(7)	0.6118(1)	1.9578(7)	4
O3	8*d*	0.0787(8)	0.2125(8)	0.2811(6)	1.9578(7)	4
O4	4*c*	0.2827(7)	0.7827(7)	0.7119(9)	1.9578(7)	2
O5	2*b*	0.000	0.5	0.2712(6)	1.9578(7)	1
x= 0.5	**$Na_{0.5}Nb_{0.1667}Ba_2Nb_5O_{15}$**					
Ba	4*c*	0.1729(6)	0.6729(6)	0.2076(1)	0.7906(1)	2
Na/Nd	2*a*	0	0	0.1900(4)	0.7906(1)	0.5/0.1667
Nb1	8*d*	0.0736(5)	0.2095(5	0.7187(3)	0.7906(1)	4
Nb2	2*b*	0	0.5	0.7077(1)	0.7906(1)	1
O1	8*d*	0.0136(1)	0.6534(8	0.7852(5)	1.2118(2)	4
O2	8*d*	0.0717(8)	0.8498(3	0.6163(8)	1.2118(2)	4
O3	8*d*	0.0795(8)	0.2105(5	0.3037(3)	1.2118(2)	4
O4	4*c*	0.2817(2)	0.7817(2	0.7024(9)	1.2118(2)	2
O5	2b	0	0.5	0.2940(5)	1.2118(2)	1
x= 0.7	**$Na_{0.3}Nb_{0.233}Ba_2Nb_5O_{15}$**					
Ba	4*c*	0.1730(8)	0.6730(8)	0.1552(2)	0.6645(5)	2
Na/Nd	2*a*	0	0	0.0794(5)	0.6645(5)	0.3/0.233
Nb1	8*d*	0.0740(3)	0.2086(3)	0.6672(1)	0.6645(5)	4
Nb2	2*b*	0	0.5	0.6785(7)	0.6645(5)	1
O1	8*d*	0.0097(9)	0.6506(3)	0.6932(1)	1.0912(2)	4
O2	8*d*	0.0645(7)	0.8535(5)	0.5787(2)	1.0912(2)	4
O3	8*d*	0.0765(4)	0.2034(6)	0.2702(5)	1.0912(2)	4
O4	4*c*	0.2832(2)	0.7832(1)	0.6324(3)	1.0912(2)	2
O5	2*b*	0	0.5	0.3148(7)	1.0912(2)	1

Table 3 Selected inter-atomic distances (Å) in the series $Na_{1-x}Nd_{x/3}Ba_2Nb_5O_{15}$

Composition	0.3	0.5	0.7
4*c* site with Coordination number = 15			
2*Ba—O1	2.846(3)	2.585(4)	2.600(5)
2*Ba—O1	2.846(4)	3.138(4)	3.149(2)
4*Ba—O2	3.242(4)	3.222(7)	3.291(7)
2*Ba—O3	3.413(3)	3.452(6)	3.457(5)
2*Ba—O3	3.169(2)	3.199(6)	3.215(1)
2*Ba—O4	2.945(5)	2.880(1)	2.798(9)
1*Ba—O4	3.067(5)	3.144(6)	3.154(3)
<Ba—O4>	3.0985	3.1031	3.1175
2*a* site with coordination number 12			
8*Na/Nd—O2	2.874(2)	2.876(8)	2.816(4)
4*Na/Nd—O3	2.847(3)	2.775(9)	2.720(5)
<Na/Nd—O>	2.8651	2.8431	2.7841
8d site with coordination number 6			
Nb1—O1	1.937(3)	1.966(6)	2.058(9)
Nb1—O2	1.955(4)	1.944(9)	2.007(2)
Nb1—O2	2.045(4)	1.978(7)	1.899(7)
2*Nb1—O3	1.991(8)	1.989(4)	1.987(1)
Nb1—O4	2.024(8)	1.970(1)	2.000(6)
<Nb1—O>	1.991	1.973	1.990
2*b* site with coordination number 6			
4*Nb2—O1	1.988(8)	2.036(8)	1.903(1)
2*Nb2—O5	1.991(1)	1.989(1)	1.985(7)
<Nb2—O>	1.989	2.021	1.931

3.3. Raman analysis

At room temperature $Ba_2NaNb_5O_{15}$ is orthorhombic (C_{2v}) with eight formula units per unit cell, consequently, there are 552 normal modes. The high temperature ferroelectric phase is tetragonal(C_{4v}) with probably two formula units per primitive cell and 138 normal modes. [29]. In our case, the structural study has shown that the A_2 sites are occupied by two different cations Na^+ and Nd^{3+} while A_1 cavities are filled only by Ba^{2+}. Indeed, all C-sites are totally empty and $B_1$and B_2 are occupied by Nb. The number of modes could be reduced to 120 Raman active optical phonon modes at zero wave vectors. The irreducible representation associated with the corresponding point group 4*mm* in this case is given by:

$$\Gamma_{(vibr)} = 19A_1+14B_1+18B_2+35E$$

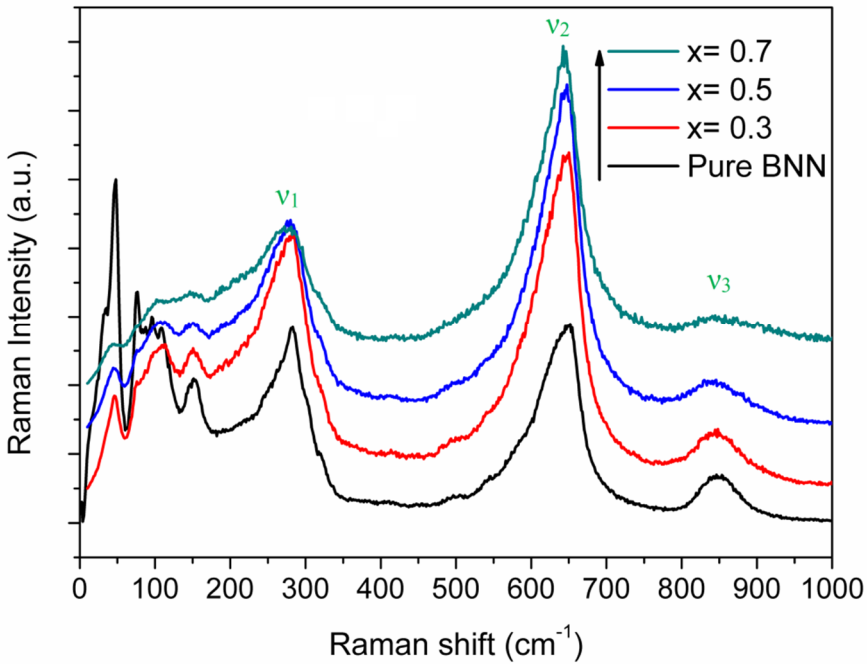

Figure 4. Raman spectra of $Ba_2(Na_{1-x}Nd_{x/3})Nb_5O_{15}$ ceramics at room temperature. The BNN spectrum is given for comparison.

As evidenced in Figure 4, the experimental results show three vibration bands situated at 270(v_1), 650(v_2), and 850(v_3) cm^{-1}, characteristic of the vibrations within the octahedral $[NbO_6]^{7-}$[30-33].Inhomogeneous broadening of the Raman lines could be attributed to a structural disorder as a result of overlapping of different Raman vibration modes. The (v_1) and (v_2) originate from $A_1(z)$, transverse optical bands, and related to O-Nb-O bending and Nb-O stretching vibration mode respectively[34]. Bodou and Sapriel [35] reported that (v_3) is assigned to $A_1(z)$ longitudinal optic mode (LO) which is attributed to the internal vibration mode of oxygen octahedra.

Obviously, the influence of the doping with Nd^{3+} is clearly seen in the region below 200 cm^{-1}. The intense mode observed for NBT at 48 cm^{-1}, decreased with the introduction of Nd^{3+}. In addition, BNN- modes at 76, 95 and 108 cm^{-1}, are overlapped on a broad one gradually with the incorporation of Nd^{3+}. Such behavior is compatible with the results reported by Noiret *et al.*[36] and corroborate our structural study.

3.4. Dielectric and energy storage study

Fig.5a represents a typical plot of the thermal variations of dielectric constant ε_r'(T) and dielectric loss at three different frequencies (10 kHz, 100 kHz, 1MHz) for the composition x=0.3. As it can be seen from the plots, ε_r'(T) exhibits abroad dielectric peak centred at 475°C, compatible with a phase transition usually attributed to a ferroelectric- paraelectric (*F-P*) phase transition. Moreover, high dispersive behaviour was observed in the frequency, it confirms the inhomogeneous grain size shown in SEM images. No clear relaxor behavior could be depicted form these plots, but the increasing of dielectric loss in paraelectric phase characterise electrical conductivity in this compound.

The ferroelectric-paraelectric phase transition was reported to appear at 580°C in BNN, whereas incommensurate phases appear between 270°C and 300°C [19]. As it can be seen from the dielelectric plots, the incorporation of 30% ofNd^{3+} in the BNN-matrix suppresses the incommensurate phases and stabilizes the tetragonal phase. This result is in good agreement with the literature [16]. As soon as the Nd^{3+} concentration increased to 50%, both the maximum value of the dielectric constant and the *F-P* transition temperature (T_c) decreased and the incommensurate phases disappear. The changes are totally compatible with most of compositional solid solution behavior.

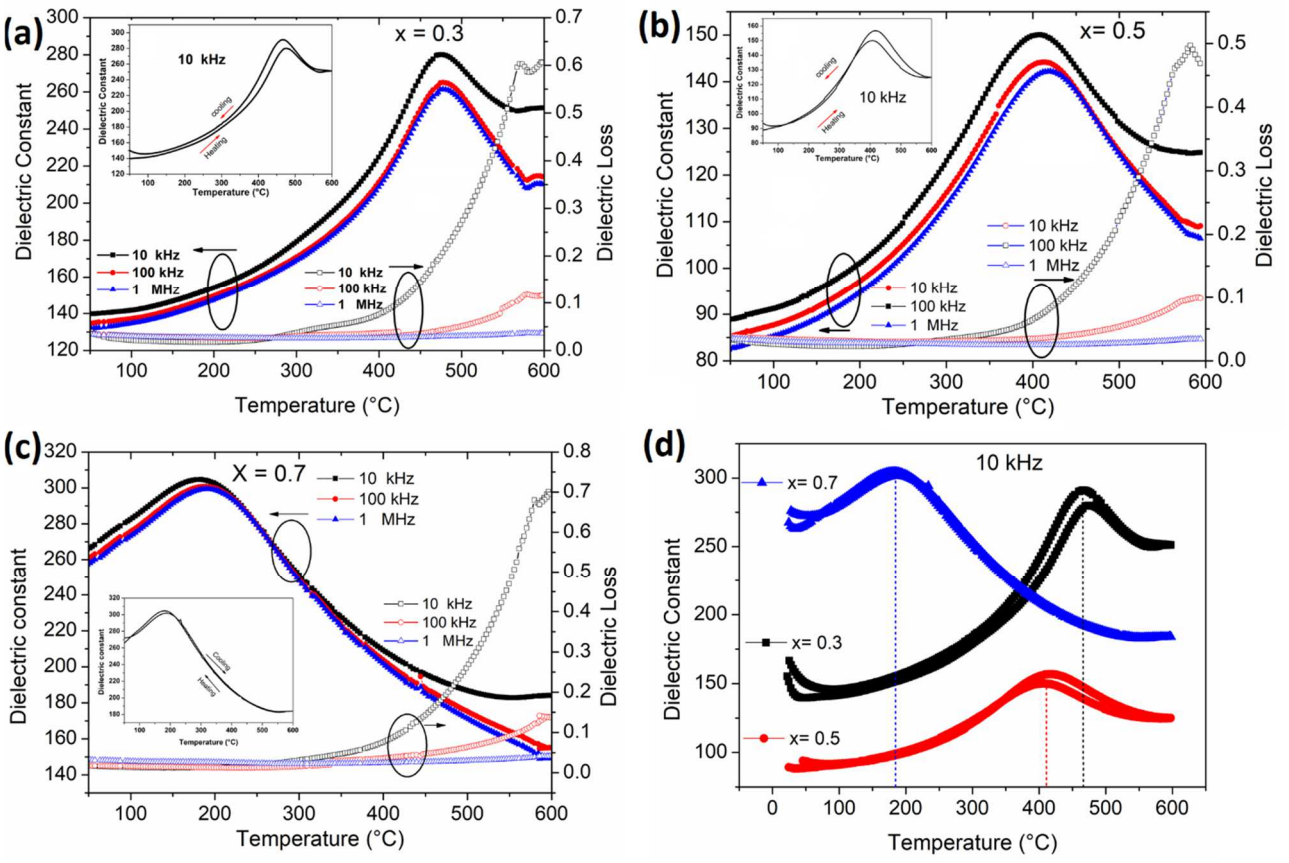

Figure 5. *(a) Temperature dependence of the dielectric constant and loss factor of* $Ba_2(Na_{1-x}Nd_{x/3})Nb_5O_{15}$ *at different Nd concentrations:(a) =0.3; (b) =0.5; (c) x=0.7; (d) comparison of dielectric constant of the three investigated samples at 10 kHz.*

Surprisingly, for x = 0.7, a drastic change is depicted with an abrupt enhance of the dielectric constant value accompanied by a depression of T_c under 200°C. As a matter of fact, such behavior could be linked to the presence of the $BaNb_2O_6$ as secondary phase.

This latter, may play a key role in the improvement of the microstructure thus the density of the ceramic, which influence widely the enhancement of the maximum of the dielectric constant and ferroelectricity. In addition, the beneficial effect of this secondary phase could be related also to the physical properties that endorsed $BaNb_2O_6$. In fact, it is reported (both hexagonal and orthorhombic polymorphic phases) as a good dielectric material (as well as ferroelectric) for microwave application [37]. The improvement of ferroelectricity could be linked also to the A sites order/disorder and the radius difference between A1 and A2-sites, which reported by Zhu *et al.* as two factors influencing the phase transition and ferroelectricity of TTB-type materials [38].

In the following we will focus the study on ferroelectric behavior and the calculation of the energy storage density in the samples. Indeed, this density is equal to the area between the horizontal axis of saturated polarization and the *P-E* hysteresis is loops, using the following equation:

$$Wrec = \int_{Pr}^{Pmax} EdP$$

Noting that there is a part of unrecoverable stored energy expressed by:

$$Wloss = \int_{-Pr}^{Pr} EdP$$

where W_{rec} represents the recoverable or stored energy, E is the applied electric field, P_{max} is the maximum of the polarization and P_r is the remnant polarization.

The energy efficiency is an important parameter that can be evaluated using the equation:

$$\eta = \frac{W_{rec}}{W_{rec} + W_{loss}} \times 100$$

Figure 6 shows the *P-E* hysteresis loops of $Ba_2(Na_{1-x}Nd_{x/3})Nb_5O_{15}$ (x = 0, 0.3, 0.5 and 0.7) at room temperature under a maximal electric field of 31.5 KV/cm, that can be reached using our experimental device. Noting that with this weak field, we failed to reach saturation of the *P-E* cycles. Even though, we have tried to calculate the energy storage properties, in such conditions, and see the influence of the introduction of Nd^{3+} on this property. In Table 4 we gathered the obtained results. As we can conclude, W_{rec} increases gradually with the composition as well as W_{loss}. The composition with small amount of Nd^{3+} (x= 0.3) exhibits lower loss and good enough efficiency compared to the other compositions.

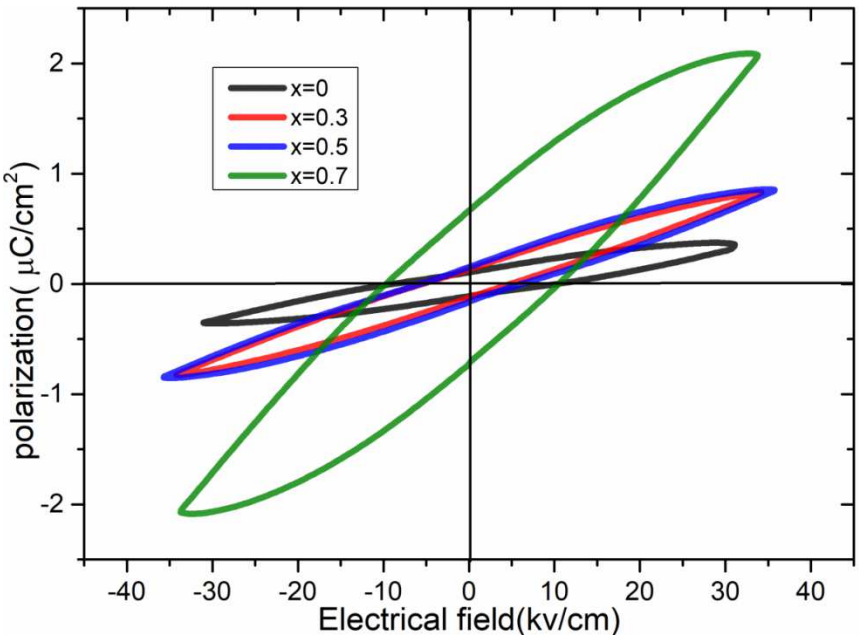

Figure6. Room temperature P-E hysteresis loop of $(Na_{1-x}Nd_{x/3})Ba_2Nb_5O_{15}$ ceramics recorded at 1kHz.The parent phase BNN is given for comparison.

Table 4: Comparison of the energy storage properties obtained in the present work with some literature data.

Composition	E (kV /cm)	W_{rec} (mJ.cm^{-3})	W_{loss} (mJ.cm^{-3})	η (%)	Refs
$Ba_{0.85}Ca_{0.15}Zr_{0.1}Ti_{0.9}O_3$	8.75	10.40	6.96	59.90	[39]
$Ba_{0.85}Ca_{0.15}Zr_{0.1}Ti_{0.9}O_3$	7.77	10.61	6.06	63.65	[39]
$Ba_{0.85}Ca_{0.15}Zr_{0.1}Ti_{0.9}O_3$	6.89	6.66	4.02	62.36	[39]
$Ba_{0.975}La_{0.017}(Zr_{0.05}Ti_{0.90})$ Sn0.05O3	12	65	43.33	60	[40]
$Ba_{0.85}Ca_{0.15}Zr_{0.1}Ti_{0.9}O_3$	6.5	14	3.5	80	[41]
$25Bi_2O_3$-25BaO-$200P_2O_5$-$97.5BaTiO_3$	15	6.9	2.6	72.58	[42]
$75Bi_2O_3$-75BaO-$600P_2O_5$-$92.5BaTiO_3$	15	2.3	3.1	42.27	[42]
2BaO-$0.5Na_2O$- P_2O_5-$2Nb_2O_5$-$0.2WO_3$	90	16.6	2.6	86.39	[43]
$BaTiO_3$	25	87	85	50.6	[44]
$BaZr_{0.05}Ti_{0.95}O_3$	50	218	84	72	[45]
$BaZr_{0.1}Ti_{0.9}O_3$	30	500	--	--	[46]
$BaZr_{0.05}Ti_{0.95}O_3$	50	218	84	72.2	[45]
$Na_{0.5}Ba_{0.5}TiO_3$	80	190	0.37	33.92	[47]
$BaTi_{0.7}Zr_{0.3}O_3$	CS 40	120	56.47	68	[48]
	SPS 170	510	188	73	
$Ba_2NaNb_5O_{15}$ (x=0)	31.5	3.1	6	34.13	This work
$Ba_2(Na_{0.7}Nd_{0.1})$ Nb_5O_{15} (x=0.3)	31.5	8	4.9	61.66	This work
$Ba_2(Na_{0.5}Nb_{0.1667})$ Nb_5O_{15} (x=0.5)	31.5	7	6.6	51.14	This work
$Ba_2(Na_{0.3}Nd_{0.233})$ Nb_5O_{15} (x=0.7)	31.5	15.1	30.2	33.41	This work

3.5. Phase transition approach by Raman investigation

The thermal variation of the Raman spectra recorded for x=0.5 within the temperature range 25°C- 1100 °C is given in Fig.7a. As can be seen from these plots, remarkable line broadening took place with increasing temperature. The same observation has been also reported by Amira et al. [49]. In addition, ν_1 and ν_2 show blue shift with increasing temperature. Besides, modes situated at low frequency are temperature dependent and seem to disappear with increasing temperature. As shown in figure 5b, this mode merged together and disappeared between 440°C and 540 °C, simultaneously with the disappearance of the band (ν_3) developed around 840 cm^{-1}. Such behaviour

is compatible with the phase transition evidenced by the dielectric investigations in this range of temperature. Furthermore, the thermal variation of the peak position (wavenumber of the peak) of both v_1 and v_2 shows also as significant deviation from linearity in the zone of phase transition, as can be evidenced in Figs.7 (c) and (d), which may constitute further support of the existence of the phase transition depicted by dielectric measurements around 450°C for x=0.7.

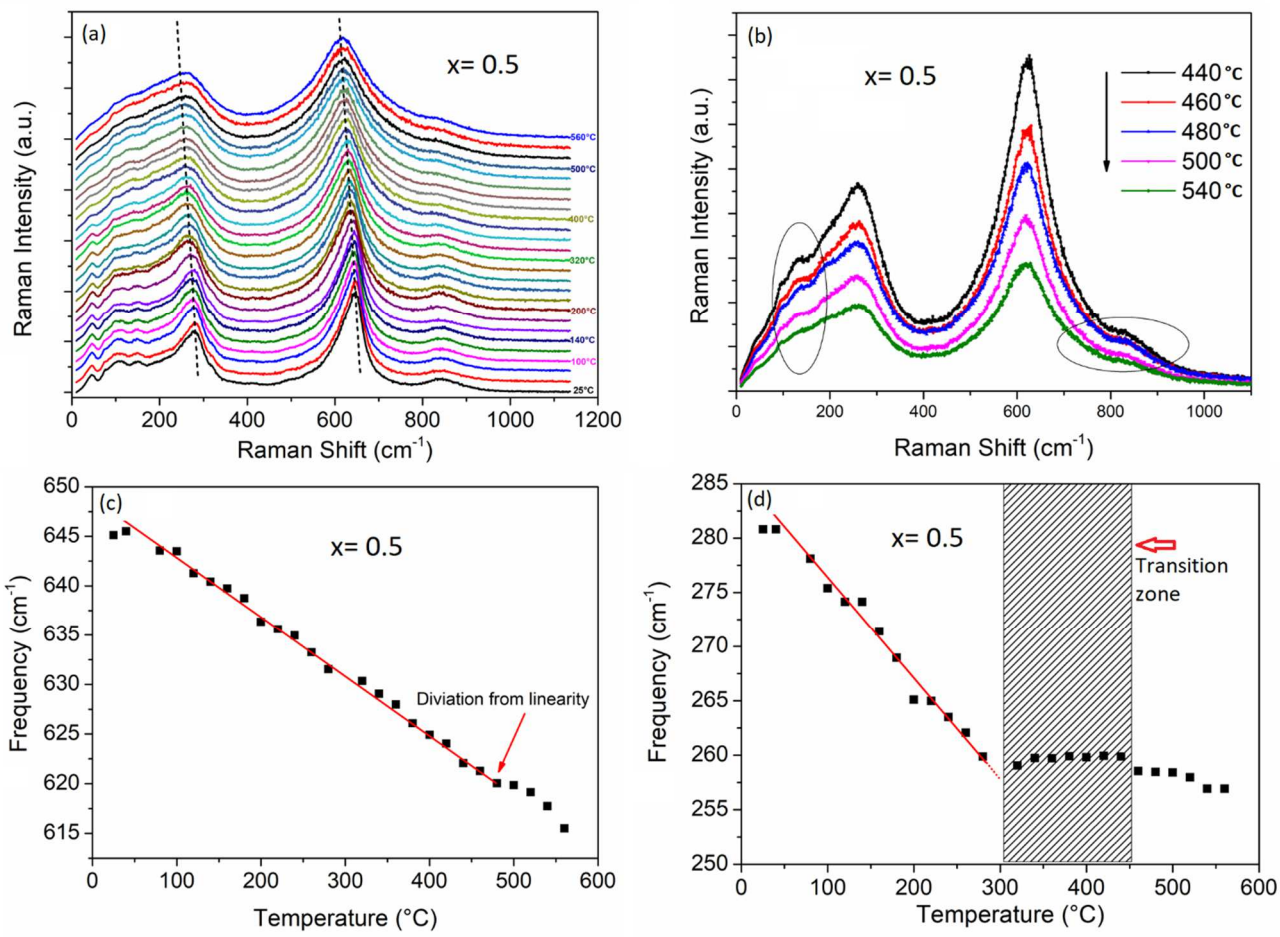

Figure 7. (*a) Thermal variation of Raman spectra* of $Ba_2(Na_{0.5}Nb_{0.1667})Nb_5O_{15}$ (x=0.5), the vertical lines are guides for the eyes to show the bleue shift of the modes ; (*b) Temperature zoom spectra showing the changes in the transition zone. (c) Variation of the peak position of v_2 mode versus temperature showing deviation from linearity in the Tc zone; (d) Variation of the peak position of v_1 mode versus temperature showing deviation from linearity in the Tc zone.*

Moreover, the phase transition in the composition x=0.7, which is observed around 200 °C is also approached by Raman investigations as a function of temperature. Figure 8 (a) shows the variation of spectra versus temperature. Recall that with increasing the Nd^{3+} content, the modes at lower wavenumber overlap and form a large one at room temperature that makes it difficult to follow the position of this band with increasing temperature. Thus, we are interested only to the v_2 mode centred around 650 cm^{-1}, which seems to be the most appropriate to probe the phase transition in the

title compound. The variation of band position of the ν_2 mode is plotted in fig.7b. The position seems to not change considerably until 120°C, then an abrupt decrease is detected at 180°C, followed by a stabilization of the peak position. This typical behavior is observed exactly in the phase transition zone that agrees well with the dielectric investigations.

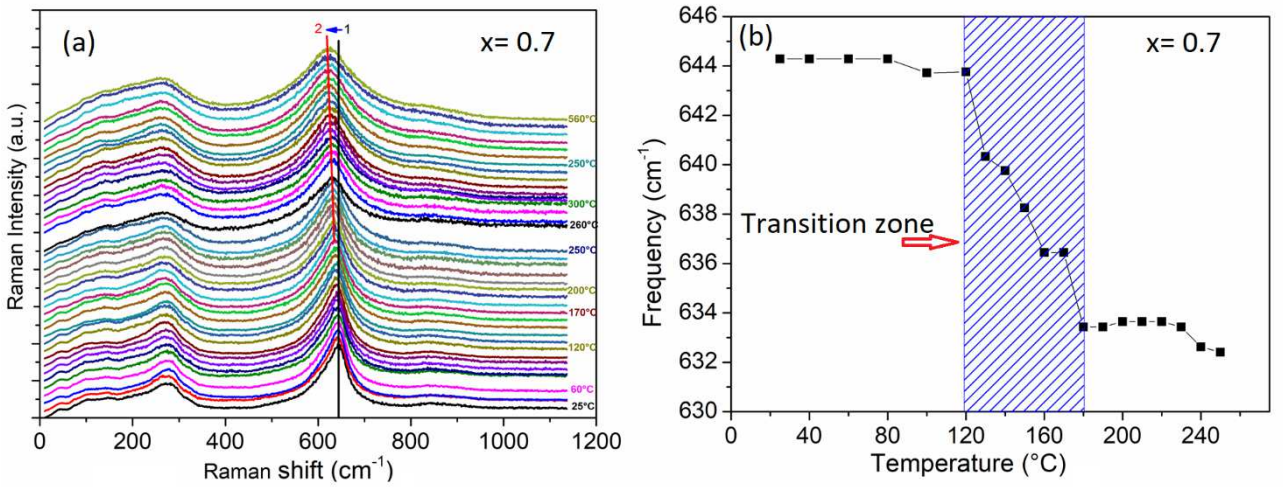

Figure 8.*(a) Variation of Raman spectra*as a function of temperature for $Ba_2(Na_{0.3}Nb_{0.233})Nb_5O_{15}$ (x=0.7), the lines are guides for theeyes ;*(b) Variation of the peak position of v_2 mode versus temperature showing deviation from linearity in the Tc zone.*

4.Conclusion

Ceramic samples with the general formula$Ba_2Na_{1-x}Nd_{X/3}Nb_5O_{15}$were prepared by solid state conventional method. The structural investigation revealed that all the samples crystallized in Tetragonal Tungsten Bronze structure. Raman investigation results confirmed that the incorporation of Nd^{3+}in BNN matrix induces a structural transition to the tetragonal one with the apparition of disordered structure on square and octahedral sites.

Furthermore, the dielectric study showed that the presence of Nd^{3+} in $BaNaNb_5O_{15}$host lattice induced the suppression of the incommensurate phase transitions. In addition, only the ferroelectric- paraelectric phase transition was observed and found to decrease with the Nd^{3+} concentration. Room temperature energy storage study showed very week values because of the unsaturated *P-E* hysteresis loops, albeit, small amount of Nd^{3+} seems to be beneficial for energy efficiency compared to the parent phase.

High temperature Raman spectroscopy, carried out versus temperature, has confirmed the existence of a thermal change within the same range of the temperature transition, that was depicted also by dielectric measurements.

Acknowledgments

This work has been carried out with the support of the "Program Hubert Curien" (PHC-Tassili No. 18MDU107/39978VH).

References

[1] M.E. Lines and A.M. Glass, Principles and applications of ferroelectrics and related materials, Clarendon Press, Oxford,1977.

[2] V. S. Filip'ev, Y. AE. Cherner, Z.V. Bondarenko and E. G. Fesenko, Phase transitions in $A_2Pb_4Nb_{10}O_{30}$ ferroelectrics with a tetragonal tungsten bronze-type structure, Solid state physics 28, 1338 (1986).

[3] B.N. Savenko, B. Sangaa, F. Proket, Neutron diffraction studies on $SrxBa_{1-x}Nb_2O_6$ single crystals with x = 0.75, 0.70, 0.61, 0.50 and 0.46, Ferroelectrics 107, 207 (1990).

[4] M.J. Ravez, A. Perron-Simon, B. Elouadi, L. Rivollan and P. Hagenmuller, Evolution de quelques propriétés physiques de phases de structure "bronzes de tungstène quadratiques" par remplacement de l'élément Alcalino-Terreux par le plomb, J. Phys. Chem. Solids 37, 949 (1976)

[5] J. Ravez and B. Elouadi, Couplage ferroelastique-ferroelectrique dans les phases de structure "bronzes de tungstene quadratiques." Mat. Res. Bull 10, 1249 (1975).

[6] P.V. Lenzo, E.G. Sencer and A.A. Balman, Electro-Optic Coefficients of Ferroelectric Strontium Barium Niobate. Applied Physics Letters, J. Appl. Phys. Lett. 11, 23 (1967).

[7] S.C. Abraham, P.B. Jamison and J.L. Bernstein, Ferroelectric tungsten bronze-type crystal structures. III. Potassium lithium niobate $K_{(6-x-y)}Li_{(4+x)}Nb_{(10+y)}O_{30}$, J. Chem. Phys. Lett 54, 2355 (1971).

[8] A.M. Glass, Investigation of the electrical properties of $Sr_{1-x}Ba_xNb_2O_6$ with special reference to pyroelectric detection, J. Appl. Phys. 40, 4699 (1969).

[9] N.Wakiya, J. K. Wang, A.Saiki, K. Shinozaki and N. Mizutani, Synthesis and dielectric properties of $Ba_{1-x}R_{2x/3}Nb_2O_6$ (R: rare earth) with tetragonal tungsten bronze structure, J. Eur. Ceram. Soc 19, 1071 (1999).

[10] H.F. Cheng, G.S. Chiou, K.S. Liu and I. N. Lin, Ferroelectric properties of $(Sr_{0.5}Ba_{0.5})Nb_2O_6$ thin films synthesized by pulsed laser deposition, Appl. Surf. Science 113-114, 217 (1997).

[11] K S. Singh, R. Sati and R.N.P. Choudhary, Synthesis and dielectric properties of $Ba_3NaRNb_{10}O_{30}$ [R= La and Sm], Pramana 38, 161 (1992).

[12] K. S. Singh, R Sati and R.N.P. Choudhary, X-ray, scanning electron microscopic and dielectric properties of ferroelectric $Ba_2Na_3RNb_{10}O_{30}$ (R= La or Sm) ceramics, J. Mater. Science Letters 11, 788 (1992).

[13] R N P. Choudhary, S. Bera, K.S Singh, and R. Sati, Structural and dielectric properties of $Ba_3NaRNb_{10}O_{30}$ (R= Nd and Gd), Indian journal of Pure and Applied Physics 31, 738 (1993).

[14] Chin Ting, Shao Xiaohong, X.U. Yuhuan and Chen Huanchu, Raman spectra of KNSBN crystals at the ferroelectric-paraelectric phase transition, Ferroelectrics 82, 37 (1988).

[15] M. Ganne, M. Dion, G.A. Fatsea and C. Levy-Clement, Etudes optique et magnétique des phases M2IMIIIM5VO15 (MI= Na, K, Rb, Cs; MIII= Nd, Eu; MV= Nb, Ta) et spectroscopie Mössbauer (151Eu), Ann. Chim. Fr.11, 95 (1986).

[16] G. Foulon, M. Ferriol, A. Brenier, Marie-Th. Chohen –Adad, M. Boudeulle, G. Boulon, Nonlinear single-crystal fibers of undoped or Nd^{3+}-doped niobates: growth by LHPG, spectroscopy and second harmonic generation,Optical Materials 8, 65 (1997).

[17]K. Lebbou, H. Itagaki, A. Yoshikawa, T. Fukuda, F. Carillo-Romo, G. Boulon, A. Brenier and M.Th. Cohen-Adad, Effect of Yb^{3+} content on purity and crystal growth of $Ba_2NaNb_5O_{15}$, J. Crystal Growth 210,655 (2000).

[18] B.A. Scott, E.A. Giess, G. Burns and D.F. O'Kane, Alkali-rare earth niobates with the tungsten bronze-type structure, Mat. Res. Bull. 3,831 (1968).

[19] J. Ravez, A. Perron-Simon, P. Hagenmuller, . Les phases de structure "bronzes de tungstèn quadratiques" : règles cristallochimiques, relations entre propriétés ferroélectriques et distorsions structurales Ann. Chim 1, 251 (1976).

[20] Y Gagou, D Mezzane, N Aliouane, T Badeche, M Elaatmani, MH Pischedda and Pi Saint-Gregoire, A new ferroelectric compound: $PbK_2LiNb_5O_{15}$, Ferroelectrics 254,197 (2001).

[21]A Lahmar, H Ehrenberg, E Antic-Fidancev, S Ganschow, M Zriouil, B Elouadi, Single crystal structure determination and infrared fluorescence of the system $(K_3Sr_{1-x}Nd_x)(Nd_{1-x}Sr_{1+x})Nb_{10}O_{30}$, Materials Research Bulletin 47,2566 (2012).

[22] J-M Reau, B.Elouadi, J.Ravez, P.Hagenmuller, Influence de la Substitution Tungstène-Niobium sur les Propriétés Cristallographiques et Diélectriques de la Solution Solide de Compositions Limites $Ba_{2.5-x}Na_{2x}Nb_5O_{15}$ ($0,23 \leq x \leq 0,60$). Le Système $BaNb_2O_6$-$(NaNbO_3)_2$-$(WO_3)_2$ à 1050°C, J. Solid State Chemistry 15, 18 (1975).

[23] J. Herrero-Albillos, P. Marchment, E. K. H. Salje, M. A. Carpenter, and J. F. Scott; Elastic behavior associated with phase transitions in incommensurate $Ba_2NaNb_5O_{15}$, Phys. Rev. B 80,214112 (2009).

[24] Enrico Cavalli, Gianluca Calestani, Enrico Bovero, Alessandro Belletti and Andrea Migliori, Optical spectra of Nd^{3+} in niobates of the tetragonal tungsten bronze family, J. Phys.: Condens. Matter 16,729 (2004).

[25] A. Boultif, D. Loueer, and D. Louër, "Indexing of powder diffraction patterns for low-symmetry lattices by the successive dichotomy method," J. Appl. Crystallogr. 24, 987–993(1991).

[26] R. D. Shannon, "Revised effective ionic radii and systematic studies of interatomic distances in halides and chalcogenides, Acta Crystallogr. Sect. A32, 751–767 (1976).

[27] J. Rodriguez-Carvajal, FULLPROF 2000: A Rietveld Refinement and Pattern Matching

Analysis Program. 2008.

[28] T. Roisnel and J. Rodríquez-Carvajal, WinPLOTR: A Windows Tool for Powder Diffraction Pattern Analysis, Mater. Sci. Forum 378–381,118–123 (2001).

[29] L. C. Bobb, I. Lefkowitz, L. Muldawer, Raman spectra of $Ba_2NaNb_5O_{15}$, Ferroeleetrics 2, 217(1971).

[30]R. Clarke and D. Siapkas, Temperature-dependent Raman spectra of ferroelectric potassium strontium niobate , J. Phys. C: Solid State Phys. 8, 377 (1975).

[31]G. Burns, J. D. Axe, D. F. O'Kane, Raman measurements of $NaBa_2Nb_5O_{15}$ and related ferroelectrics, Solid State Communications 7, 933 (1969).

[32] H. R. Xia, H. Yu, H. Yang, K. X. Wang, B. Y. Zhao, J. Q. Wei, J. Y. Wang, Y. G. Liu, Raman and infrared reflectivity spectra of potassium lithium niobate single crystals Phys. Rev. B 55, 14892 (1997).

[33] H-R. Xia, L-X. Li, H. Yu ,X-L. Meng, L. Zhu and L-J. Hu, Raman and infrared spectra of Nd-doped barium sodium niobate crystals, Cryst. Res. Technol. 34, 901 (1999).

[34] G. Burns, J. D. Axe, D. F. O' Kane, Raman measurements of $NaBa_2Nb_5O_{15}$ and related ferroelectrics, Solid State Communications 7, 933 (1969).

[35] A. Boudou and J. Sapriel, Raman-scattering investigations in tetragonal tungsten bronze compounds. I. $Ba_2NaNb_5O_{15}$ and related crystals, Phys. Rev. B 21,61 (1980).

[36] I. Noiret, J. Schamps, J. Lamiot, G. Boulon and A. Brenier, Phase transitions in the 5 at.% Nd^{3+}-doped $Ba_2NaNb_5O_{15}$ self-doubling laser crystal, Phys. Rev.B 69, 104110 (2004).

[37] D.W Kim, H.B Hong, K.S Hong, C.K Kim, D.J Kim. The Reversible Phase Transition and Dielectric Properties of $BaNb_2O_6$ Polymorphs, Jpn J Appl Phys.41(10R), 6045 (2002).

[38] X.L. Zhu, K. Li, X.M. Chen
Ferroelectric transition and low-temperature dielectric relaxations in filled tungsten bronzes
J Am Ceram Soc, 97 (2) (2014), pp. 329-338, 10.1111/jace.12790

[39] H. Mezzourh, S. Belkhadir, D. Mezzane, M. Amjoud, E. Choukri, A. Lahmar, et al. Enhancing the dielectric, electrocaloric and energy storage properties of lead-free $Ba_{0.85}Ca_{0.15}Zr_{0.1}Ti_{0.9}O_3$ ceramics prepared via sol-gel process, Phys B : Condens. Matter.603, 412760 (2021).

[40] S. Smail, M. Benyoussef, K. Taïbi, N. Bensemma, B. Manoun, M. El Marssi, A. Lahmar, Structural, dielectric, electrocaloric and energy storage properties of lead free $Ba_{0.975}La_{0.017}(ZrxTi_{0.95-x})Sn_{0.05}O_3$ (x = 0.05; 0.20) ceramics, Mater. Chem. Phys. 252, 123462 (2020).

[41] Z. Hanani, D. Mezzane, M. Amjoud, A. Razumnaya, S. Fourcade, Y. Gagou, et al., Phase transitions, energy storage performances and electrocaloric effect of the lead-free $Ba_{0.85}Ca_{0.15}Zr_{0.10}Ti_{0.90}O_3$ ceramic relaxor, J. Mater. Sci. Mater. Electron.30(7), 6430–8 (2019).

[42] E. Haily, L. Bih, A. El bouari, A. Lahmar, M. El Marssi, B. Manoun, Effect of $BaO–Bi_2O_3–P_2O_5$ glass additive on structural, dielectric and energy storage properties of $BaTiO_3$ ceramics, Mater. Chem. Phys.241, 122434 (2020).

[43] A. Ihyadn, A. Lahmar, D. Mezzane, L. Bih, A. Alimoussa, M. Amjoud, et al., Structural, elelectrical and energy storage properties of $BaO–Na_2O–Nb_2O_5–WO_3–P_2O_5$ glass–ceramics system, Mater. Res. Express.6, 115203 (2019).

[44] T. Wang, X. Wei, Q. Hu, L. Jin, Z. Xu, Y. Feng, Effects of $ZnNb_2O_6$ addition on $BaTiO_3$ ceramics for energy storage, Mater. Sci. Eng B. 178, 1081-6 (2013).

[45] T. Badapanda, S. Chaterjee, A. Mishra, R. Ranjan, S. Anwar, Electric field induced strain, switching and energy storage behaviour of lead-free Barium Zirconium Titanate ceramic, Phys B: Condens. Matter.521, 264-9 (2017).

[46] Y. Zhang, Y. Li, H. Zhu, Z. Fu, Q. Zhang, Sintering temperature dependence of dielectric properties and energy-storage properties in $(Ba,Zr)TiO_3$ ceramics, J. Mater. Sci. Mater. Electron.28, 514-8 (2017).

[47] M. Zanne, J. Belhadi, M. Benyoussef, H. Khemakhem, K. Zaidat, M. El Marssi, A. Lahmar, Electrostatic energy storage in antiferroelectric like perovskite, Superlattices Microstruct. 127, 43-8 (2019).

[49] B. Liu, Y. Wu, YH. Huang, KX. Song, YJ. Wu, Enhanced dielectric strength and energy storage density in $BaTi_{0.7}Zr_{0.3}O_3$ ceramics via spark plasma sintering, J. Mater. Sci. 54, 4511-7 (2019).

[49] Y. Amira, Y. Gagou, A. Menny, D. Mezzane, A. Zegzouti, M. Elaatmani and M. El Marssi, Structural and Raman properties of the tetragonal tungsten bronze ferroelectric $Pb_{2(1-x)}K_{1+x}Gd_xNb_5O_{15}$, Solid. Stat. Comm. 150, 419 (2010).